ELSEVIER

Journal of South American Earth Sciences 19 (2005) 399–414

Journal of
South American
Earth Sciences

www.elsevier.com/locate/jsames

Volcanological and geochemical evolution of the Diamante Caldera–Maipo volcano complex in the southern Andes of Argentina (34°10′S)

Patricia Sruoga[a,*], Eduardo J. Llambías[b], Luis Fauqué[c], David Schonwandt[c], David G. Repol[d]

[a]*CONICET—Servicio Geológico Minero Argentino. Av. J. A. Roca 651,10, Capital Federal (1322), Argentina*
[b]*CONICET—Universidad Nacional de La Plata. Calle 1 644, La Plata, 1900, Argentina*
[c]*Servicio Geológico Minero Argentino. Av. J. A. Roca 651,10, Capital Federal (1322), Argentina*
[d]*Department of Geology and Geophysics, University of Calgary, Canada*

Accepted 15 June 2005

Abstract

Two main stages are distinguished in the evolution of the Diamante Caldera–Maipo volcano complex. The 'Diamante stage' corresponds to the emplacement of large volume rhyolitic ignimbrites associated with a 20×16 km diameter collapse caldera. This ~0.45 Ma catastrophic event was followed by the 'Maipo stage,' which represents the last 100 ka of the complex's lifetime. Fieldwork and Ar/Ar data support an eruptive record within the Maipo stage that consists of at least four pre-last glacial maximum (pre-LGM) large volume events and three postglacial small volume events. Historic activity remains uncertain. At present, neither fumarolic activity nor hydrothermal manifestations are detected. Dominantly effusive, the Maipo stage includes blocky and flow-banded lavas, a ring-fault dome, and subordinate pyroclastic deposits that define a high-K, calc-alkaline suite ranging in silica from 53 to 68% and encompassing two pyroxene with minor olivine andesites and two pyroxene and hornblende-bearing dacites. Within the volcanic complex, a general geochemical trend toward more evolved, potentially higher explosive products is recognized. Differentiation is strongly controlled by fractional crystallization, but disequilibrium textures suggest periodic magma mixing must be significant in the production of cyclic chemical variations.

Keywords: Diamante caldera; Geochemistry; Maipo volcano complex; Southern Andes; Volcanological evolution

1. Introduction

The Diamante Caldera–Maipo volcano complex (DMC) is located at 34°10′ south latitude in the Andean Cordillera on the border between Argentina and Chile. The Maipo volcano, 5323 m high, was emplaced in the western portion of the Diamante caldera. At present, the two summit craters remain covered in ice. The lack of fumarolic or hydrothermal activity and an uncertain historic record turns this volcano suspiciously quiet compared with neighboring volcanic centers like San José and Tupungatito.

According to Siebert and Simkin (2002), four historic eruptions may be attributed to the activity of the Maipo volcano. However, González Ferrán (1995) admits a more expanded historic record, including at least eight eruptions between 1822 and 1912 and a probable last event in 1931. He also attributes a postglacial age to the whole Maipo volcanic cone, whereas Harrington (1989) argues that a small dome, emplaced along the ring fracture zone, represents the only postglacial Maipo volcanic activity.

Within this controversial and confusing framework, fieldwork supported by Ar/Ar data establishes a preliminary eruptive stratigraphy for the eastern side of the Maipo volcano (Sruoga et al., 1998, 2000). However, the main difficulty remains in identifying any conclusive evidence of historic activity.

This article focuses on the volcanological and geochemical evolution of the DMC by highlighting both the compositional characteristics of each eruptive event and

* Corresponding author. Tel.: +54 11 4349 3134; fax: +54 11 4349 4114.
E-mail addresses: psruog@minproduccion.gov.ar (P. Sruoga), patysruoga@yahoo.com.ar (P. Sruoga).

0895-9811/$ - see front matter © 2005 Elsevier Ltd. All rights reserved.
doi:10.1016/j.jsames.2005.06.003

the general chemical trend as a function of time. The main purpose of this study is to contribute to the hazard assessment of the Maipo volcano using a petrological approach.

2. Tectonic and geologic setting

The DMC belongs to the northern section of the southern volcanic zone (SVZ), which extends continuously from 33 to 46°S (Fig. 1a). Located 300 km from the oceanic trench, it represents the easternmost eruptive center of this Andean segment (Fig. 1b) and overlies the 18–20° dipping Wadati–Benioff zone (Stauder, 1973; Barazangui and Isacks, 1976). The SVZ is commonly divided in three segments: a northern section (NSVZ: 33–34.5°S), characterized by thicker continental crust and more silicic magmas than the transitional section (TSVZ: 34.5–37°) and the southern section (SSVZ: 37–46°) (Frey et al., 1984; López Escobar, 1984; Hildreth and Moorbath, 1988; Tormey et al., 1991).

The geologic evolution of the region began tentatively in the Devonian. Low-grade metamorphic rocks, known as Lagunitas Formation, are distributed throughout the Cordillera Frontal. During the Permo-Triassic, the emplacement of the volcanoplutonic Choiyoi Group took place. The Mesozoic records extensive sedimentation in marine and continental environments related to global eustatic changes. During the Cenozoic, variations in the tectonic framework and the reorganization of the stress field led to the Andean orogeny, which was accompanied by synorogenic deposits and related arc-backarc volcanism. The distribution of the main stratigraphic units in the surrounding area of the DMC appears in Fig. 2.

The oldest Mesozoic rocks correspond to the stable shelf limestones of the Oxfordian La Manga Formation, according to the well-preserved remains of Inoceramus sp. (Bühler et al., 1996). The overlying gypsum and finely interbedded limestones of the Auquilco Formation represent a shallow, restricted marine environment. This unit constitutes the main structural detachment level of the Mesozoic sequence during the Andean orogeny. The end of the sedimentary cycle in the Late Oxfordian was caused by a diastrophic event reflected in the Araucanian unconformity (Stipanicic and Rodrigo, 1970). Sedimentation continued with the deposition of conglomerates and sandstones in a fluvial environment, known as the Tordillo Formation of Kimmeridgian age. This unit records deposition in an intra-arc basin during a sea level lowstand (Legarreta and Gulisano, 1989). Tordillo red beds interfinger westward with andesitic and basaltic flows and thick polimictic breccias that belong to the Rio Damas Formation.

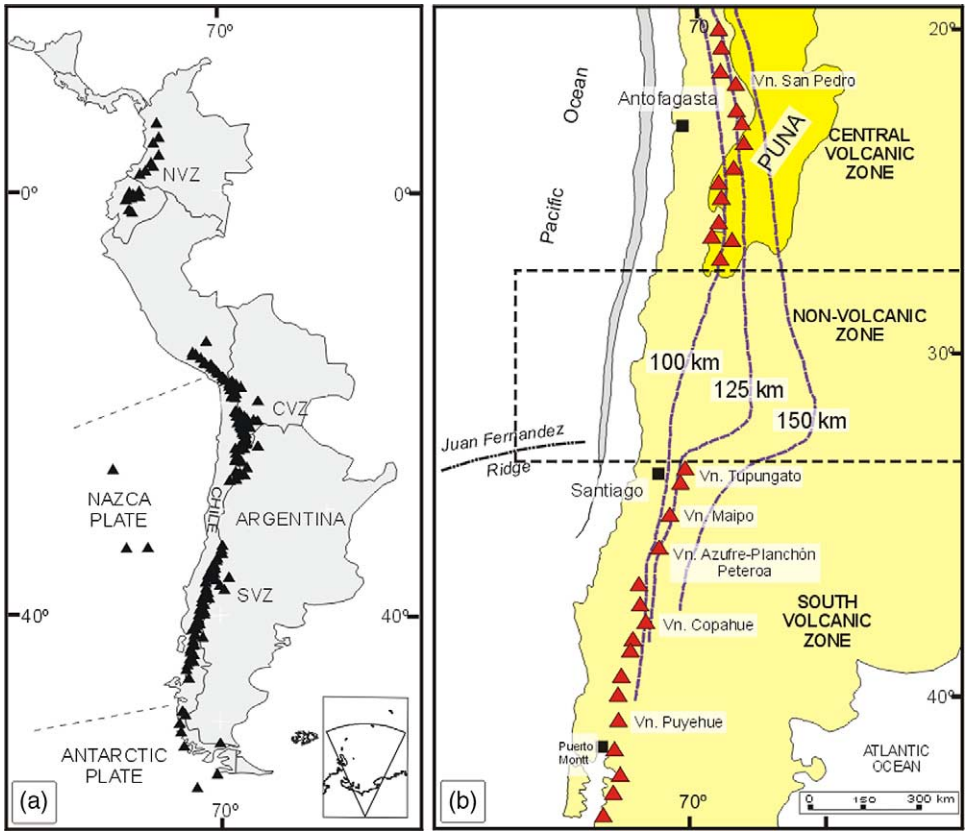

Fig. 1. Tectonic setting. (a) The SVZ is shown in relation to the central and northern volcanic zones of the South American Andes. (b) The location of the Maipo volcano is shown in relation to other eruptive centers that define the present magmatic arc. A nonvolcanic zone (28–33°S), resulting from a flat slab tectonic regime since Miocene times, separates the SVZ and CVZ.

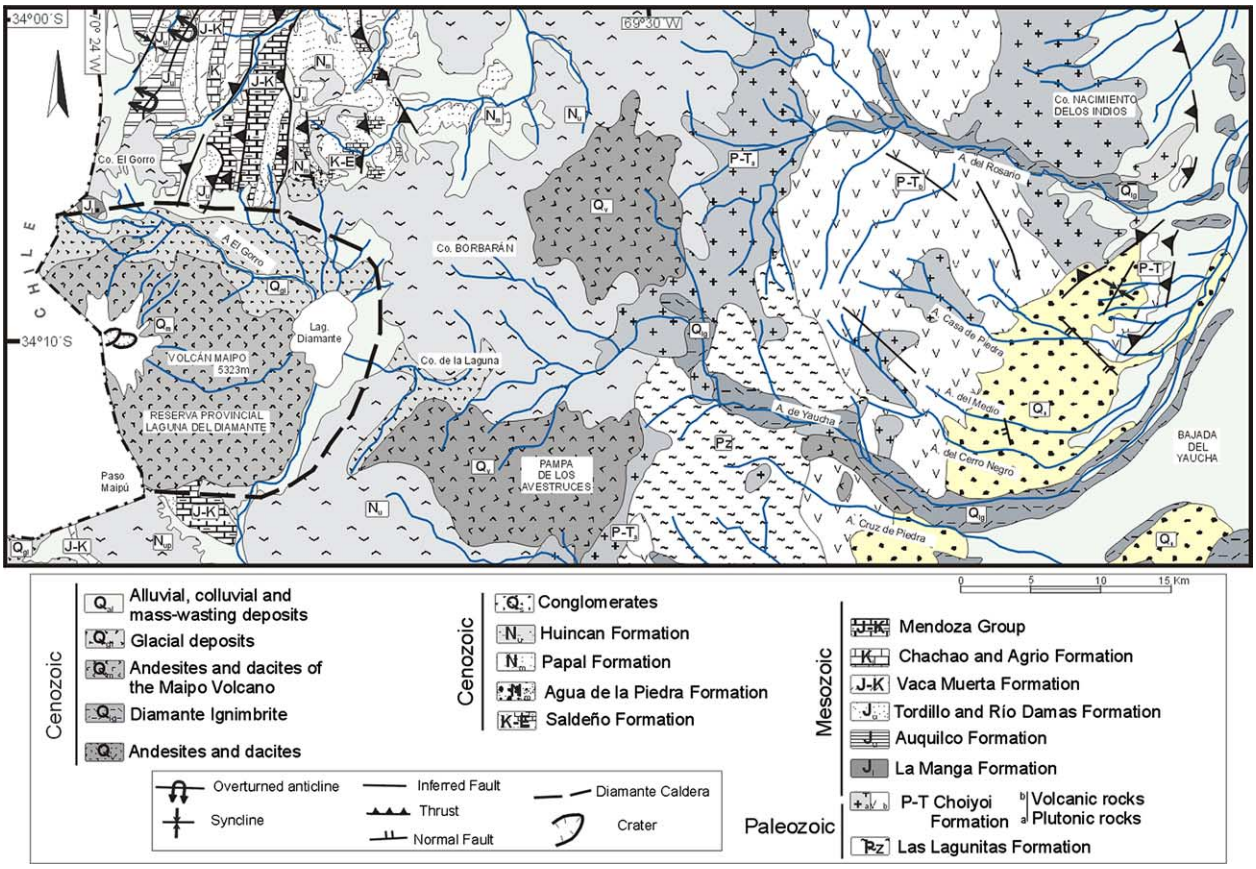

Fig. 2. Geologic and geomorphologic map of the Andean segment containing the DMC. Main geographic locations referred to in the text are included. Modified from Sruoga et al. (1998).

According to Charrier (1984), two magmatic arcs were active between Kimmeridgian and Aptian times.

Near the end of the Jurassic, a renewed sea level highstand period followed by a lowstand period led to the deposition of the Mendoza Group. In this part of the Neuquen Basin, the Mendoza Group is represented by the Vaca Muerta, Chachao, and Agrio Formations. The upper Tithonian Vaca Muerta Formation includes clay, clayish micrites, and rich-organic matter micrites that record a distal marine environment with periodic changes in depth. The Chachao Formation consists of thick *Exogyra couloni*-bearing limestone beds. Tithonian–Late Valanginianin in age, this unit was deposited in a carbonatic shelf environment. Finally, the Agrio Formation is composed of micritic limestones and coquina banks with abundant marine invertebrates of a coastal environment. According to Legarreta et al. (1993), major eustatic changes with two flooding peaks occurred after the Late Valanginian–Late Hauterivian. The upper portion of the Mezosoic sedimentary record has been cut off by late, out-of-sequence thrusts.

The end of the Cretaceous is characterized by a significant inversion in the subsidence trend that reflects either a proto-cordillera uplift (Ramos, 1988) or the inception of an Andean-type volcanic arc (Legarreta and Uliana, 1991). The Maastrichtian Saldeño Formation records the first Atlantic transgression and definitive disconnection with the Pacific Ocean (Legarreta et al., 1993).

During the Cenozoic, the so-called Andean orogeny was responsible for the Aconcagua fold and thrust belt. This antithetic, thin-skinned, folded belt extends from the San Juan River in the north to the Diamante River in the south (Ramos et al., 1998) and was active during the Miocene, though in the Pliocene, the deformation progressed eastward and resulted in the Frontal Cordillera uplift. Due to basement involvement during deformation, the Maipo area may be considered a transition zone between the Aconcagua and the Malargüe fold-and-thrust belts. The latter resulted from the inversion of a Jurassic extensional system during the Tertiary. The associated synorogenic deposits are represented by the dominantly conglomeradic Agua de la Piedra Formation, of middle Miocene age. This unit is correlated with the Tunuyán conglomerate, which is widely extended north of the study area. The Papal Formation likely also constitutes a thick synorogenic sequence of evaporites, marls, sand, and silt deposits. According to Pérez et al. (1997), this unit records a hipersaline lake sporadically connected to the Atlantic Ocean during the middle Miocene.

Fig. 3. Panoramic view of the Maipo volcano from the eastern wall of Diamante caldera. The Laguna Diamante is in the foreground, and the western topographic margin of the Diamante caldera may be seen at the background.

The associated calc–alkaline magmatism is represented by dacitic porphyries and andesitic and dacitic lava flows assigned to the Huincan Formation of Miocene–Pliocene age. The only available geochronological data remain unpublished (Bühler, 1997). Cerro El Gorro andesites have been dated at 14 ± 0.5 Ma and a nearby granodioritic porphyry at 4.2 ± 0.6 Ma. At the upper northern caldera wall, lava flows rest unconformably over Mesozoic rocks. Locally, at Enumeradas creek, these lava flows are flexured due to normal faulting related to the major collapse caldera. The existence of pre-caldera stratovolcanoes between the Late Miocene and Pleistocene is evidenced by a succession of lava flows, ignimbrites, and lahar deposits at Cerro de la Laguna. Although geochronological data are lacking in this area, volcanic activity may be considered uninterrupted since the Late Miocene.

The pre-caldera units are exposed at the northern caldera wall. An east-vergent set of thrusted Mesozoic sedimentary rocks are intruded by subvolcanic bodies and covered by lava flows of Mio–Pliocene age.

3. Volcanic stratigraphy

Two main stages are envisaged for the evolution of the DMC: the 'Diamante stage' that corresponds to the emplacement of large volume ignimbrites and the related, collapsed Caldera Formation and the 'Maipo stage' that corresponds to the construction of an andesitic–dacitic stratovolcano.

3.1. Diamante stage

The formation of the Diamante caldera, 20×16 km in diameter, took place ~ 0.45 Ma ago (0.47 ± 0.07–0.44 ± 0.08 Ma, Stern et al., 1984). The collapse resulted from the evacuation of 270–350 km^3 (DRE = 135–170 km^3) of rhyolitic, non- to moderately welded ignimbrites (Guerstein, 1990). This unit, known as 'Asociación Piroclástica Pumícea' (Polanski, 1964) and 'Diamante Tuff' (Harrington, 1989), extends widely in Chile and Argentina and covers an area of 23,000 km^2 (Stern et al., 1984). In Chile, main outcrops are recognized along the Maipo, Cachapoal, and Rapel Andean valleys, in the Central Depression, and underneath the cities of Rancagua and Santiago (Stern et al., 1984). In Argentina, Guerstein (1993) determined the propagation area between the town of Pareditas to the north and the Diamante River, located 60 km to the south. The ignimbritic flows traveled mainly along the Yaucha, Rosario, and Papagayos valleys (Fig. 2), generating a widespread pyroclastic plain in the northern foothills of Mendoza. The outcrops are discontinuous southward, whereas eastward, they disappear under modern gravel deposits.

According to Guerstein (1993), the Asociación Piroclástica Pumícea includes two basal fall deposits and a main dense ash-flow deposit. The lowest 4 m, thick ash and lapilli deposit is overlain by another relatively thin ash-fall deposit. The main ash-flow deposit represents a single cooling unit, 200 m thick in the valleys and 10 m thick in the plain. Although it may be classified as a nonwelded ignimbrite, it locally exhibits moderately welded zones. They are high-K rhyolites with plagioclase, quartz, sanidine, biotite, and scarce hornblende as the main mineral assemblage (Guerstein, 1993). This large-volume, low-temperature ($T < 600$ °C) ignimbritic eruption would represent a short and catastrophic event with an estimated VEI of 7 (Guerstein, 1993).

3.2. Maipo stage

During post-caldera reactivation and after a long nonvolcanic period (~ 350 ka), the construction of the Maipo stratovolcano occurred (Figs. 3 and 4). On the Argentine side, seven eruptive events have been identified during the last 100 ka of this stage. Table 1 shows the Ar/Ar data for the pre-last glacial maximum (pre-LGM) record (Sruoga et al., 2000), whereas the postglacial sequence is based on field observations.

Most Maipo volcanic activity took place during the last glaciation interval, which spans 90 and ~ 14 ka (Clapperton, 1993). During this large interval, several fluctuations were recorded, the most significant of which, the Global Last Glaciation Maximum, occurred at ~ 20–14 ka and is very well constrained in the southern Lake District, Chile (Denton et al., 2000). For the area of study, there is neither glacial stratigraphy nor dating available. In the upper Mendoza River (33°S), Argentina, the last glaciation is

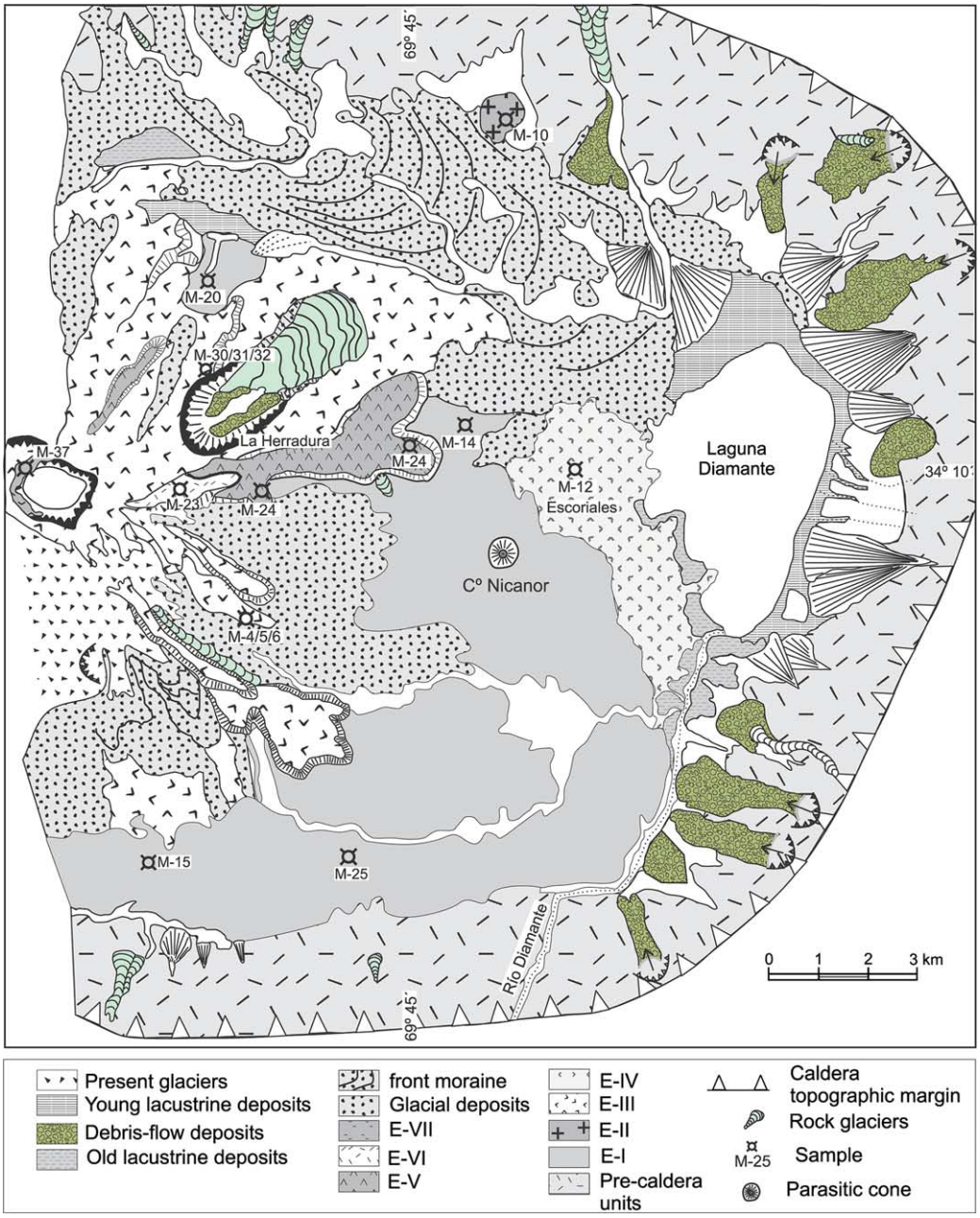

Fig. 4. Geologic and geomorphologic map of the Maipo volcano in the Argentine side. Modified from Sruoga et al. (1998). Volcanic stratigraphic sequence is shown (see text for explanation).

represented by the Penitentes drift, dated at 22.8±3.1 ka (Espizúa, 1993) and correlated with Llanquihue II (Pereyra, 1996), whereas the Horcones and Almacenes drifts correspond to the late glacial interval (14–10 ka, Espizúa, 1993). Till deposits and several moraine arcs within the Diamante caldera and on Maipo slopes indicate multiple glacial fluctuations that are tentatively assigned to the LGM.

3.2.1. Eruptive event I (EEI)

The oldest lava flows are very well exposed at the bottom of the southern and eastern flanks and poorly preserved at the northern flank of the volcano (Fig. 4). They are covered

Table 1
Ar/Ar geochronology of Maipo lavas. Analyses were performed at the Geological Survey of Canada

Eruptive Event (EE)	Type	Ar/Ar Age (ka)
VII	Andesitic scoria	<14
VI	Dacitic lavas	<14
V	Dacitic lavas	<14
IV	Andesitic lava flows	28±17[a]
III	Dacitic lava flows	45±14[a]
II	Dacitic dome	75±16[b]
I	Andesitic lava flows	86±10[a]

[a] Whole rock.
[b] Biotite concentrate.

by a thin drift glacial deposit and exhibit glacial features, such as polished surfaces and striae. The porhyritic vesicular andesites are dark gray in color (Fig. 5a) and have a phenocryst content ranging 13–37%. The characteristic assemblage is plagioclase (An_{46}), ortho and clinopyroxene, apatite, and Fe–Ti oxides set in a dark brown, glassy, flow-foliated groundmass. Plagioclase is dominant (Table 2), appearing as zoned, slightly corroded, euhedral to subhedral phenocrysts. Typically, it displays sieve textured zones, either as abundant glass inclusions in crystal cores or as peripheric narrow crystal rims. Round to elongate empty vesicles are abundant. Lithic content is low and represented by a few highly altered andesitic fragments.

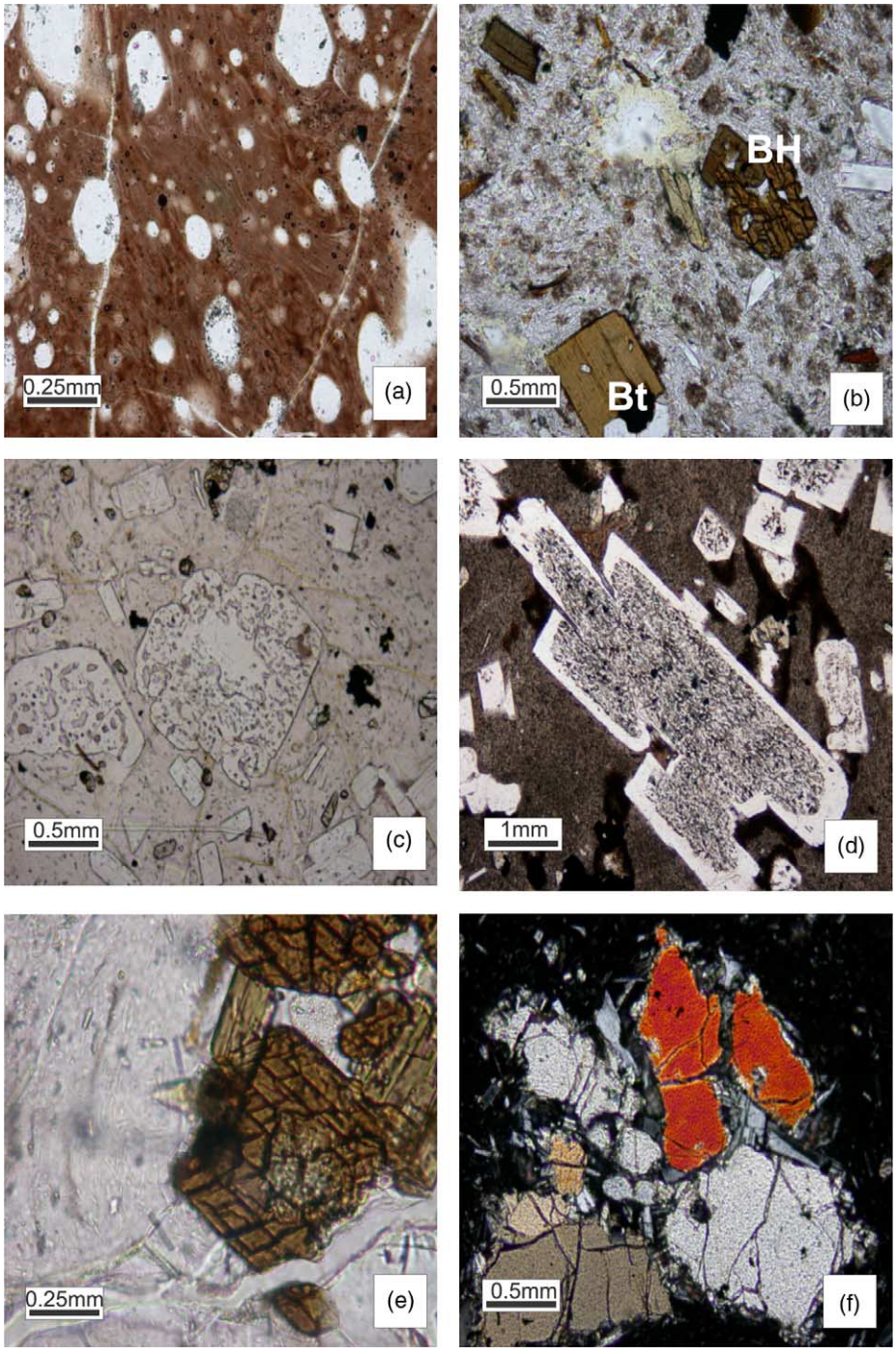

Fig. 5. Representative photomicrographs of Maipo rocks with typical disequilibrium textures (a) No. 3, 20×, vesicular flow-banded andesite, plane polarized light (PPL). (b) No. 10, 10×, basaltic hornblende (BH) and biotite (bt) set in a crystalline groundmass, PPL. (c) No. 5, 10×, glassy dacite, variably sieved plagioclase crystals, PPL. (d) No. 6, 5×, core-sieved plagioclase with clean rim, PPL. (e) No. 5, 20×, hornblende basal section set in glassy matrix with very thin opacite rims, PPL. (f) No. 31, 10×, advanced resorption in orthopyroxene aggregate, crossed nicols.

3.2.2. Eruptive event II (EEII)

A dacitic dome, located close to the northern wall of the Diamante caldera, is assigned to this event (Fig. 4). It appears as a small isolated body, with steep margins and vertical columnar jointing. According to Harrington (1989), it corresponds to a post-caldera dome emplaced in the northern ring-fault zone and has been interpreted as the only postglacial activity of Maipo volcano. However, the identification of lateral moraines on the southern flanks indicates an older age (Sruoga et al., 1998), which was confirmed by radiometric data (Table 1). Although this dome is unique, the existence of other similar bodies along the caldera ring faults is possible. Eventual discovery of equivalent domes would make this event volumetrically relevant.

Dacites are porphyritic and greenish gray, with a high content of phenocrysts (40–45%), set in a hypocrystalline groundmass, slightly altered to sericite and calcite. The main mineral assemblage consists of plagioclase, sanidine, brown hornblende, and biotite with apatite and Fe–Ti oxides as accessory phases (Table 2). Plagioclase is euhedral to subhedral, commonly zoned, rarely sieved, and rich in mafic inclusions. Sanidine is relatively abundant and appears as clear euhedral crystals. Biotite is found as small, fresh, flexured blades and contains abundant apatite and Fe–Ti oxide inclusions. Brown hornblende appears in subhedral crystals, exhibiting strong brown to reddish pleocroism. The mineral phase is unique in the volcanic suite (Fig. 5b).

3.2.3. Eruptive event III (EEIII)

This major event was responsible for most of the volcanic cone construction. Dominantly effusive, it encompasses a succession of andesitic to dacitic lava flows and minor intercalated pyroclastic deposits. The volcanic pile is very well exposed at the southern and southeastern flanks, where glacial erosion was stronger than at the northern flank. 'La Herradura,' a glacial cirque occupied by several rock glaciers (Fig. 4), offers a particularly suitable place to study the sequence of flow-banded lava flows, flow breccias, and interbedded pyroclastics. Total thickness exceeds 300 m, whereas individual flow thickness is highly variable from 2 to 25 m. Lateral geometry is roughly continuous, indicating the absence of deep channels during the outpouring of lava flows. Typically, they exhibit parallel and convolute flow banding, with alternating dark gray and reddish bands. Coarse fall deposits carry bombs of different types, mostly bread crust-types, nonvesiculated dacitic fragments, and scoria fragments of variable size.

Andesites and dacites are porphyritic with a total phenocryst content of 22–32%, including plagioclase, sanidine, ortho and clinopyroxene, minor hornblende, apatite, and Fe–Ti oxides (Table 2). Although modal proportions may change in the different lava flows, plagioclase is always dominant and displays a wide range of textural features, including sieved core crystals, entirely sieved crystals (Fig. 5c), sieved zones with a clear external rim (Fig. 5d), embayed and rounded crystals, and zoned crystals. Sanidine is always scarce and appears euhedral,

Table 2
Modal proportions of representative samples

	No.	Plg	San	Cpx	Opx	Hbl	Bt	Oliv	Fe–Ti ox	zr	ap	Ves	Phenocryst total content
EE I	M3	20		6	2				3			15	31
	M-8	15		3	1				1			8	20
	M-15	10		2	0.5				0.5			12	13
	M-20	22		3	1				1			10	27
	M-25	20		7	3			2	5			10	37
EE II	M10	23	7			8	5		1		1		44
EE III	M4	18	2	3	2	1			2		1		29
	M-5	18	1	5	3	2	0.5		2		0.5		32
	M-6	15	2	4	2	1			4		1		29
	M-7	18	1	5	4				2				30
	M-30	18	0.5	3	1				1		0.5		24
	M-31	18	1	3	1	2			1		1		27
	M-33	15	1	3	1				1		1		22
EE IV	M-12	22		7	3			2	1				35
EEV	M-13	18	1	5	2	1	1		1				29
	M-14	15	1	4	2				1			2	23
	M-24	20	1	6	4	0.5			3	0.5	0.5	2	35
EE VI	M-23	15		4	2	0.5		1	2		0.5	2	25
EE VII	M-37	10		2					0.5			30	12.5
	M-38	12		1	0.5			0.5	0.5			30	14.5

Plg, plagioclase; San, sanidine; Cpx, clinopyroxene; Opx, orthopyroxene; Hbl, hornblende; Bt, biotite; Oliv, olivine; Fe–Ti ox, Fe–Ti oxides; zr, zircon; ap, apatite; and ves, vesicles.

inclusion free, and slightly corroded. Green hornblende is tiny and rare, commonly developing thin opacite rims (Fig. 5e). Clinopyroxene shows glass inclusions and thin reaction rims and commonly is zoned and rounded (Fig. 5f). A late euhedral orthopyroxene is recognized within the resorbed main crystal of orthopyroxene (Fig. 6a). Phenocrysts frequently form glomeroporphyritic aggregates of one or more phases. The groundmass ranges from colorless glassy with perlitic zones to finely crystalline. Diorite lithic fragments are exceptional.

3.2.4. Eruptive event IV (EEIV)

The blocky lava flows found at the lower eastern flank of the volcano are known as 'escoriales del Maipo' (Fig. 4). These lavas have high, steep flow fronts and are only partially covered by drift deposits. Tentatively, they are

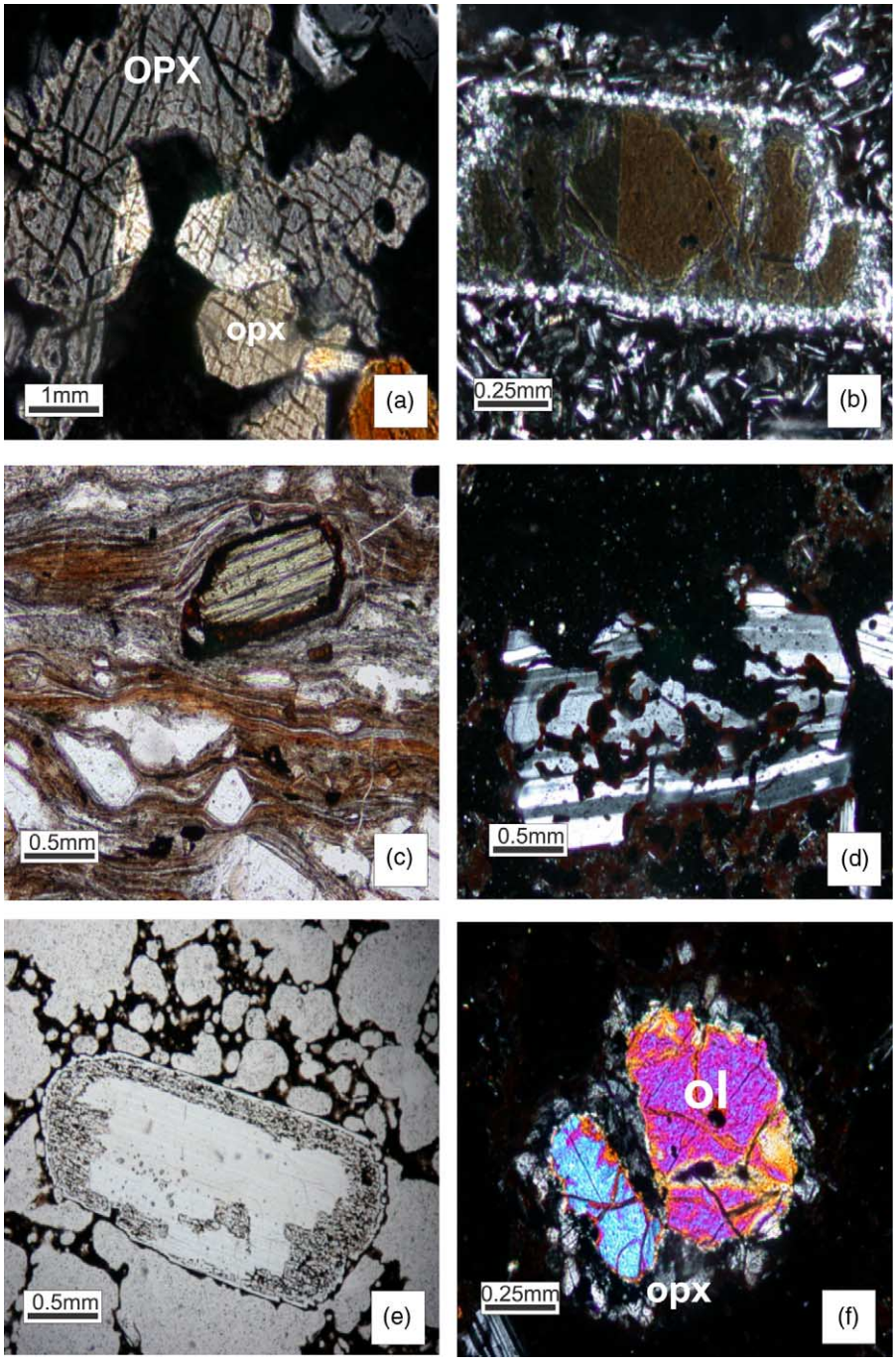

Fig. 6. Representative photomicrographs of Maipo rocks with typical disequilibrium textures (a) No. 6, 5×, partially resorbed orthopyroxene (OPX) and late euhedral pyroxene (opx).Crossed nicols. (b) No. 12, 20×, embayed orthopyroxene with reaction rim. Crossed nicols. (c) No. 24, 10×, flow-banded dacite, resorbed orthopyroxene, PPL. (d) No. 38, 10×, advanced corrosion in plagioclase. Crossed nicols. (e) No. 37, 5×, scoria fragment, peripheric sieve texture in plagioclase, PPL. (f) #38, 20×, reaction rim in olivine (ol), surrounded by orthopyroxene (opx). Crossed nicols.

Table 3
Whole-rock major, trace, and rare-earth elements analysis of DMC

	Events																		
	Rhyolites	EE-I					EE-II	EE-III						EE-IV		EE-V		EE-VI	EE-VII
	M16	M3	M8	M15	M22	M25	M10	M4	M5	M6	M20	M31	M33	M12	M14	M13	M24	M23	M37
SiO_2	74.29	57.02	60.19	60.19	56.06	57.05	66.44	65.05	66.66	65.18	60.48	66.78	63.52	57.89	61.15	67.86	67.67	64.06	53.47
Al_2O_3	13.14	18.02	17.53	17.53	17.61	17.11	15.92	15.87	14.76	15.68	18.08	15.41	16.03	17.21	16.90	15.36	15.04	15.82	16.85
Fe_2O_3t	0.96	6.07	6.46	6.46	7.48	7.12	3.34	4.30	3.74	4.77	5.57	4.07	5.16	7.13	5.80	3.75	3.83	4.81	5.26
MnO	0.08	0.09	0.10	0.10	0.120	0.113	0.09	0.07	0.06	0.08	0.091	0.066	0.078	0.11	0.10	0.06	0.065	0.076	0.074
MgO	0.19	1.98	2.34	2.34	4.49	4.15	1.10	1.99	1.47	1.99	1.71	1.67	2.50	3.98	2.72	1.43	1.56	2.06	1.68
CaO	0.66	6.87	6.04	6.04	7.76	7.03	3.27	3.98	3.12	4.13	5.47	3.55	4.69	6.77	5.26	3.21	3.20	4.59	8.70
Na_2O	3.97	4.24	4.26	4.26	3.60	3.67	4.49	4.01	3.80	3.99	4.62	3.91	3.94	3.85	4.10	3.95	3.84	3.79	3.60
K_2O	4.52	2.05	2.44	2.44	1.85	1.99	3.14	3.27	3.87	3.47	2.79	3.66	3.08	2.20	2.67	3.90	3.96	3.52	2.08
TiO_2	0.12	0.93	0.96	0.96	0.948	0.948	0.48	0.64	0.51	0.64	0.917	0.600	0.731	0.91	0.81	0.53	0.520	0.656	0.849
P_2O_5	0.05	0.28	0.26	0.26	0.21	0.23	0.18	0.15	0.18	0.21	0.29	0.16	0.20	0.25	0.24	0.18	0.16	0.19	0.22
LOI	2.96	1.18	−0.04	−0.04	0.37	−0.28	1.02	−0.04	0.36	0.04	0.01	0.25	0.30	0.39	0.15	0.52	0.64	0.65	6.78
Total	100.92	98.73	100.54	100.54	100.51	99.13	99.45	99.29	98.53	100.18	100.04	100.12	100.23	100.68	99.88	100.75	100.48	100.23	99.58
Cr	16	18	21	13	60.3	54.9	13	42	32	56	−20.0	27	51	86	31	25	20.2	30.0	−20
Ni	58	−10	−10	−10	21.1	−15.0	−10	−10	−10	−10	−15.0	23	31	−10	−10	−10	−15.0	−15.0	28
Co	0.7	15	17	17	20.0	12.0	4.7	11	8.8	14	8.1	9	13	18	14	7.8	7.9	10.0	12
Ba	786	542	584	539	449	456	767	659	674	676	629	679	628	554	588	663	668	613	524
Rb	173	71	91	70	55	57	114	148	163	152	89	157	122	73	90	166	155	126	77
Th	14	12	13	10	7	8	17	21	24	21	10	18	14	11	15	25	19	17	9
U	7	4	4	3	2	2	5	7	8	7	3	6	5	3	4	8	6	5	3
Nb	15	9	11	9	7	6	10	13	14	13	10	11	10	9	10	13	12	10	8
Ta	1	1	1	1	1	1	1	1	1	1	1	1	1	1	1	1	1	1	1
La	17	28	31	27	23	24	35	36	39	38	33	43	39	28	33	39	40	36	28
Ce	34	60	62	54	48	50	68	75	81	76	66	85	78	57	67	81	78	71	59
Sr	69	537	525	562	486	446	353	377	318	406	483	348	430	516	449	329	326	359	589
Nd	13	26	29	27	22	23	26	30	30	31	29	31	30	27	28	30	29	28	24
Sm	3	5	6	5	4	5	5	5	5	6	6	6	6	5	6	6	5	5	5
Zr	91	211	212	195	152	150	224	255	262	252	196	229	213	193	221	257	235	212	170
Hf	3	5	5	5	4	4	6	6	6	6	5	6	6	5	5	6	6	6	5
Tl	1	0	0	0	0	0	1	1	1	1	0	1	1	0	0	1	2	1	5
Tb	0	1	1	1	1	1	1	1	1	1	1	1	1	1	1	1	1	1	1
Y	17	20	22	21	20	19	18	22	22	22	23	21	21	21	23	22	21	20	17
Yb	2	2	2	2	2	2	2	2	2	2	2	2	2	2	2	2	2	2	2
La	16.60	27.80	30.80	26.90	23.08	24.36	34.90	36.30	39.10	37.80	32.64	42.50	38.50	27.90	32.50	39.00	39.80	36.40	28.00
Ce	34.20	59.70	61.70	54.10	47.62	50.07	67.70	74.80	80.50	75.50	65.51	84.70	78.30	56.80	67.40	80.90	77.72	71.42	58.60
Pr	3.47	6.37	6.71	6.01	5.67	5.91	6.57	7.92	8.06	7.83	7.58	8.57	8.05	6.22	6.82	8.12	8.26	7.77	6.21
Nd	15.00	9.20	11.00	9.20	6.53	6.20	10.00	13.00	14.00	13.00	9.84	11.00	10.00	9.00	10.00	13.00	11.84	10.42	8.00
Sm	2.76	5.16	5.75	5.33	4.38	4.52	4.65	5.42	5.41	5.70	5.51	5.60	5.50	5.32	5.79	5.51	5.22	5.11	4.60
Eu	0.41	1.23	1.20	1.20	1.25	1.26	0.94	0.96	0.92	0.99	1.47	1.15	1.25	1.08	1.21	0.88	1.06	1.11	1.29
Gd	2.73	4.74	4.98	4.66	4.07	4.30	4.14	5.21	5.06	5.11	4.95	4.80	4.80	4.71	4.82	5.01	4.26	4.31	4.20
Tb	0.44	0.60	0.67	0.65	0.61	0.61	0.54	0.64	0.60	0.66	0.73	0.70	0.70	0.66	0.64	0.61	0.63	0.64	0.60
Dy	2.46	3.22	3.83	3.54	3.33	3.40	3.00	3.39	3.37	3.52	4.01	3.70	3.70	3.48	3.69	3.25	3.50	3.51	3.10
Ho	0.47	0.66	0.70	0.67	0.66	0.67	0.58	0.67	0.69	0.68	0.76	0.70	0.70	0.67	0.71	0.67	0.69	0.67	0.60
Er	1.59	1.94	2.21	2.04	1.94	1.97	1.95	2.17	2.17	2.17	2.22	2.10	2.10	2.08	2.14	2.13	2.01	1.95	1.60

Table 3 (*continued*)

	Events																	
	Rhyolites	EE-I				EE-II	EE-III					EE-IV		EE-V		EE-VI	EE-VII	
	M16	M3	M8	M15	M22	M25	M10	M4	M5	M6	M20	M31	M33	M12	M14	M13	M24	M23	M37	
Tm	0.26	0.25	0.34	0.30	0.27	0.27	0.32	0.33	0.33	0.34	0.32	0.32	0.31	0.31	0.31	0.33	0.31	0.28	0.24	
Yb	1.50	1.55	1.96	1.80	1.84	1.80	1.88	1.97	1.99	1.93	2.22	2.10	2.00	1.84	2.06	1.99	2.09	1.91	1.50	
Lu	0.22	0.25	0.28	0.26	0.27	0.27	0.30	0.29	0.32	0.30	0.32	0.28	0.28	0.27	0.30	0.31	0.32	0.29	0.21	

DS, diamante stage. Analytical procedures from Actlabs, Canada.

associated with a small parasitic scoria cone called C° Nicanor, which has a central crater and a lateral outlet. On the basis of the excellent preservation of their primary morphologic features, González Ferrán (1995) attributes these lavas to the 1826 eruption and concludes that the origin of the lake is directly related to the lava dam. However, the identification of old lacustrine deposits (Fig. 4) and the evidence of periodic high stands suggest the origin of the lake might be related to the final stages of ice melting during the last glaciation (Sruoga et al., 1998). As mentioned previously, the lava flows are partially covered by glacial drift deposits, indicating a pre-LGM age as confirmed by Ar/Ar results (Table 1).

Dark gray in color, the rocks are vesicular and porphyritic. They contain 35% plagioclase (An_{52}), ortho and clinopyroxene, and minor olivine. Plagioclase is found in two groups of different size: euhedral-zoned microphenocrysts and sieved core corroded phenocrysts (1–2 mm). Both pyroxenes commonly show zonation and signs of corrosion, such as embayment and reaction rims (Fig. 6b). The groundmass is dark brown glassy to fine crystalline.

3.2.5. Eruptive event V (EEV)

A prominent dacitic lava flow lies on the eastern flank of the Maipo volcano. Steep marginal levees bound the central channel, and the lava front bifurcates in two distal lobes (Fig. 4). The original morphology has not been affected by glacial erosion, and the lava flow lies on moraine deposits, indicating postglacial emplacement.

Fresh dacites, gray greenish in color, are porphyritic, with 29–35% total phenocryst content (Table 2), and consist of plagioclase, sanidine, ortho and clinopyroxene, and minor hornblende as the main mineral phases. They also include apatite, zircon, and Fe–Ti oxides as accessory minerals. Plagioclase is euhedral to subhedral and shows zonation and a variably developed sieve texture. Sanidine is always clear with occasional signs of corrosion. Orthopyroxene includes abundant apatite inclusions and displays conspicuous reaction rims (Fig. 6c). Hornblende, as a green type, is always present as small and scarce sections. The few lithics are biotite porphyritic fragments. The groundmass ranges from light brown and glassy with quenching fractures to flow-foliated finely crystalline.

3.2.6. Eruptive event VI (EEVI)

A very short, 2 km dacitic lava flow, distinguishable by its darker color, overlies the bilobate EEV lava flow. Small volume magma poured from the central vent and traveled a short distance along the central channel of the older lava flow. The lava front is located at 4150 m.

Petrographically, the dacite is very similar to the previous event. They are porphyritic with a 25% phenocryst content of sieved plagioclase, pyroxene, minor hornblende, apatite, and Fe–Ti oxides (Table 2) immersed in a fine crystalline groundmass.

3.2.7. Eruptive event VII (EEVII)

The basaltic andesite scoria deposits found at the summit of the volcano are interpreted as the last pyroclastic event of uncertain age. Tentatively, they are correlated with the bomb fields spread over the south-eastern flank.

The scoria fragments range in color from black to reddish gray according to their degree of oxidation. Highly vesicular, they reveal a low phenocryst content of plagioclase, ortho and clinopyroxene, and Fe–Ti oxides set in a dark glassy matrix. Plagioclase appear mostly broken, showing both sieve cores and sieve peripheric zones (Fig. 6d and e). Exceptional olivine exhibits reaction rims that consist of tiny orthopyroxene attached to the reacted crystal (Fig. 6f).

3.2.8. Historic chronology

According to Siebert and Simkin (2002), the Maipo volcano has a record of four eruptions: 1822?, 1826, 1905, and 1912. On the basis of written chronicles and geologic interpretation, González Ferrán (1995) concludes that the historic activity is more extensive, including episodes in 1788, 1829, 1831, 1833, 1869, 1908, and 1931 as well. This author describes the activity as alternating lava flow emission, scoria cone construction, strong phreatomagmatic eruption, tefra ejection, fumarolic activity, and avalanche and lahar generation. Also, González Ferrán (1995) associates "the explosions and vibrations recorded at Rancagua in 1905" to Maipo volcanic activity, which is 75 km away from that city. In contrast, Petit-Breuilh (pers. comm.) of OVDAS-SERNAGEOMIN, Chile, considers, on

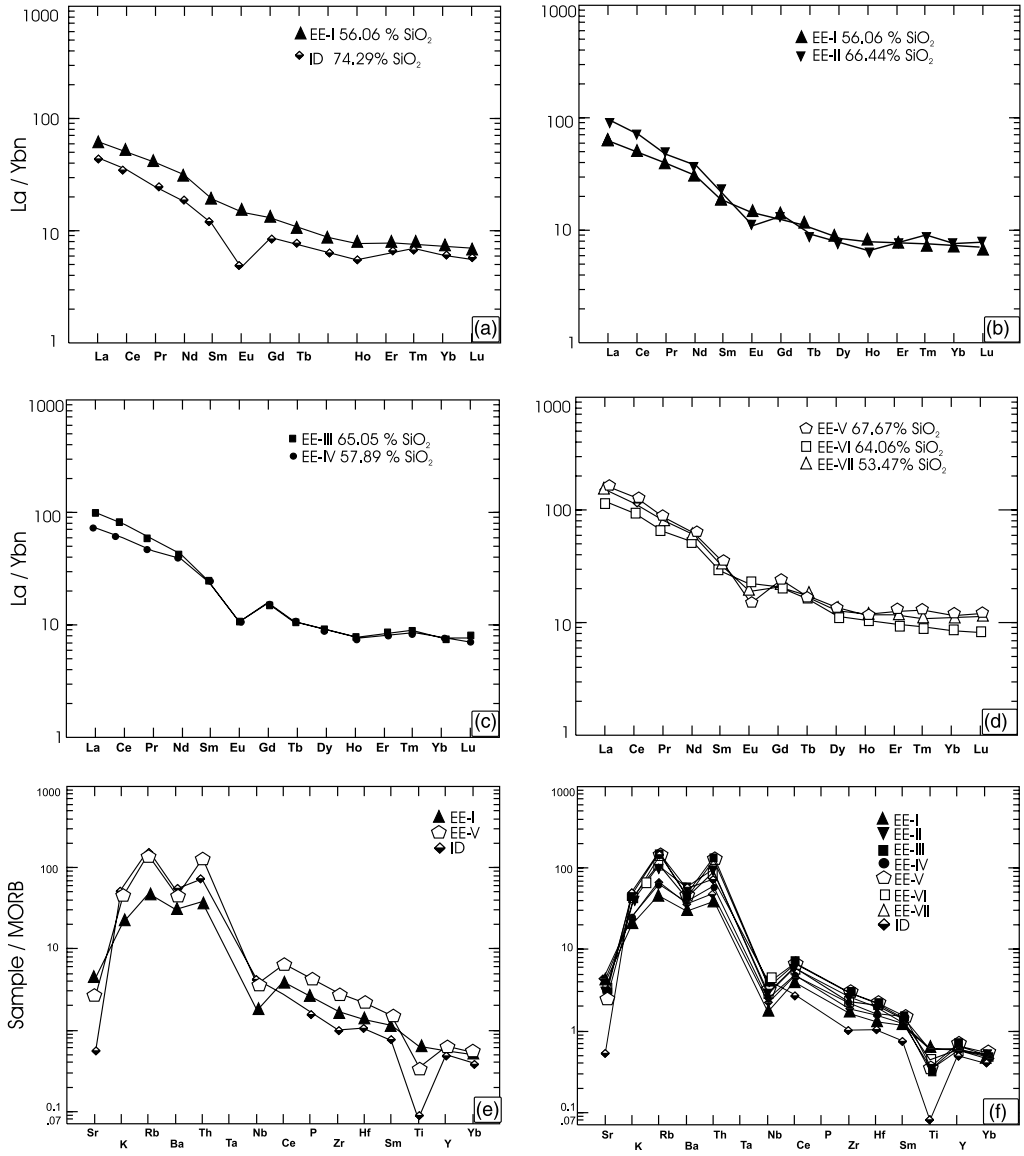

Fig. 7. (a–d) Representative REE patterns show geochemical evolution of the DMC. (e and f) Representative 'spider' plots. Normalization constants are from Taylor and McLennan (1985) and Pearce (1983). See text for discussion.

the basis of an exhaustive study of old chronicles, that the most reliable episodes occurred in 1826, 1829, 1905, and 1912, whereas those in 1822, 1831, 1833, 1835, 1837, 1869, 1881, 1908, and 1929 remain uncertain. The EEVII identified in the summit may correspond to the 1912 episode.

The main obstacle to obtain a truly reliable historic chronology lies in the ambiguity of most chronicles in the identification of the eruptive center. Part of the confusion arises from the old name of the San Jose volcano, known as San Jose del Maipo. In addition, Maipo's remote location and the lack of visual witnesses make the target difficult to achieve.

4. Geochemistry

Major and trace element whole-rock analysis for selected samples of the DMC appear in Table 3. They define a high-K, calc–alkaline suite of large compositional range (Fig. 7a and b). The entire range of silica content spans 53–74% and encompasses basaltic andesites, andesites, dacites, and rhyolites. A real 68–74% gap is detected between the most evolved Maipo dacites and the Diamante rhyolitic ignimbrites (Fig. 7a and b).

Compared with other volcanic complexes of the same Andean segment, DMC volcanics exhibit similar content in significant petrogenetic elements (López Escobar, 1984; Hildreth and Moorbath, 1988). They show Ba enrichment (524–786 ppm); Rb (57–173 ppm), Ce (34–85 ppm), and Th (7–24 ppm) depletion; and typical negative anomalies in TiO_2 (0.12–0.96%), Nb (6–15 ppm), and Hf (3–6 ppm) (Figs. 8 and 9). Likewise, the Ba/La ratios (6–17) and La/Yb (7.5–13.7) ratios are as expected for subduction-related volcanics in continental margins.

The rare earth element (REE) patterns are very useful for describing the geochemical evolution of the DMC and the differentiation mechanisms operating through time. Representative samples of each eruptive event are compared to show the main geochemical trends (Fig. 9a–d).

Diamante rhyolites represent the more evolved end-member of the whole suite. They exhibit large negative Eu anomalies and strong Sr, Nb, and Ti depletion accompanied by significant Rb, Ba, and Th enrichment (Fig. 9a, e, and f). Major and trace element behavior indicates that

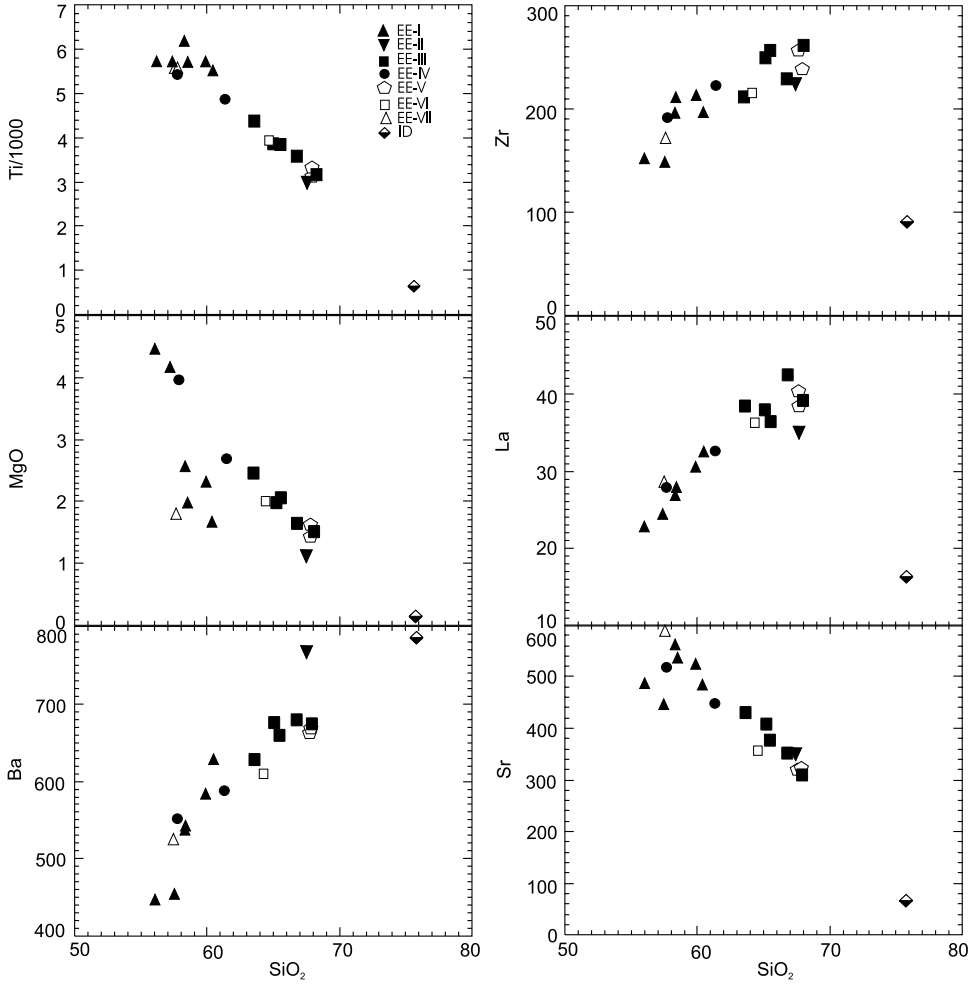

Fig. 8. Selected Harker diagrams.

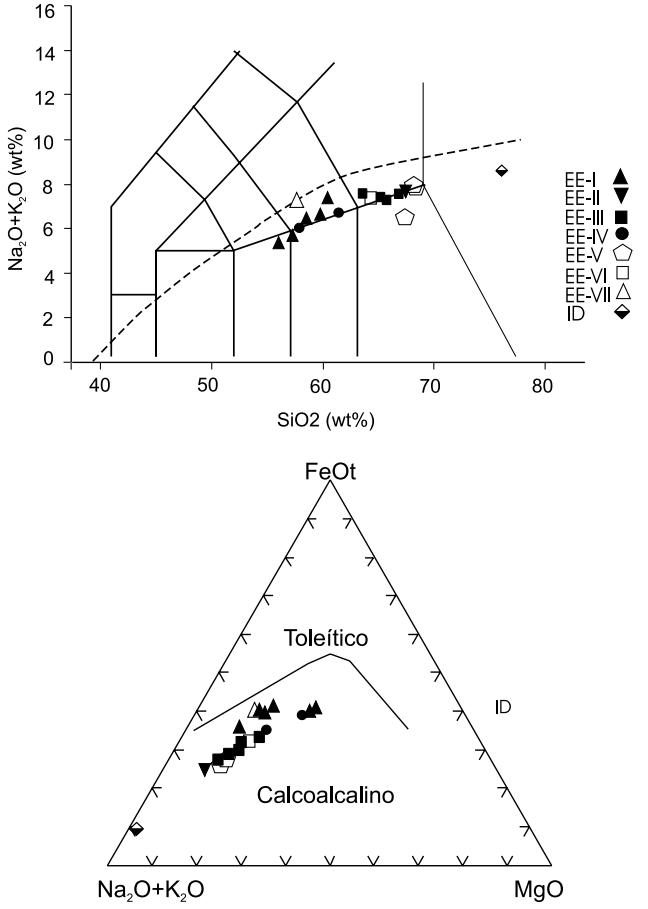

Fig. 9. (a) Total alkali-silica plot, after Le Maitre et al. (1989). Closed symbols, preglacial lavas; open symbols, postglacial lavas. DI, diamante ignimbrite. Dashed line separates subalkaline and alkaline fields, from Irvine and Baragar (1971). (b) AFM diagram, boundary between calc-alkaline and tholeiitic fields after Irvine and Baragar (1971).

differentiation was strongly controlled by fractional crystallization of plagioclase, sanidine, hornblende, biotite, apatite, and zircon. Fig. 8 shows that La and Zr behavior is controlled by zircon and probably monacite fractionation.

EEI lavas correspond to relatively low differentiated magmas, with low La/Yb ratios and no negative Eu anomaly (Fig. 9a). EEII represents the emplacement of more evolved magma batches, as reflected in the higher SiO_2 content, higher LREE, a small negative Eu anomaly, and MREE depletion, which resulted in a characteristic concave-up shape (Fig. 9b). These features are consistent with plagioclase, sanidine, and hornblende fractionation. The mineral phases have been identified optically (Table 2). EEIII lavas show REE patterns very similar to EEII (Fig. 9c), which suggests a persistent trend toward a high magmatic differentiation. In contrast, EEIV lavas represent an inversion toward less evolved terms and exhibit geochemical characteristics similar to EEI (Fig. 9c). EEV represents the high differentiation end-member among all the lavas emplaced during the Maipo stage. Together with an increase in the silica content, these dacites achieve the highest La/Yb ratios due to their LREE enrichment, MREE depletion, and the generation of a significant negative Eu anomaly (Fig. 9d). Analogous to EEII and EEIII, these features are attributed to plagioclase, sanidine, and hornblende fractionation. EEVI lavas show a less differentiated character than EEV rocks, and EEVII represents the low differentiation end-member of the whole suite.

5. Discussion

Geochronological and geochemical representative data allow the depiction of the volcanological evolution of the DMC (Fig. 10). Although further studies are necessary to assess the volcanic hazard of this eruptive center, this study may serve to constrain its future behavior in case of reactivation.

The onset of modern volcanism in this Andean region took place ~0.45 Ma ago with the catastrophic emplacement of ~350 km^3 of ignimbritic flows (Guerstein, 1990) and the formation of a collapse caldera due to rapid magma withdrawal from a shallow (4–7 km, Lipman, 2000) magmatic chamber. In the evolution of the DMC, the Diamante stage was paroxysmal and geologically instantaneous. It took ~350 ka for the magmatic system to achieve a new petrological equilibrium, according to the construction of a dominantly effusive stratovolcano. The Maipo stage records relatively large volume pre-LGM activity with mainly central-vent lava eruptions, small volume postglacial activity, and few uncertain episodes in historic times (Fig. 10a).

The earliest post-caldera lavas of the Maipo stage were emplaced 86 ka ago. These two-pyroxene andesites represent the arrival of the first batch of intermediate magma after a 350 ka period of volcanic quiescence. Then, 75 ka ago, magma emplacement shifted to the northern caldera ring fault zone. The brown hornblende and biotite-bearing dacitic dome, though small in volume, is significant because it represents a differentiation trend controlled by the fractionation of plagioclase and hydrous mineral phases. After 30 ka, Maipo reactivation resulted in the outpouring of large viscous dacitic lava flows. These flow-banded, two-pyroxene with hornblende dacites constitute the main cone-building episode and suggest suitable conditions for long-lasting magma differentiation. Finally, 28 ka ago, volcanic activity shifted from the central vent to a parasitic cone on the eastern flank and produced blocky lava flows of two pyroxenes with olivine and a return to more mafic compositions.

The construction of Maipo stratovolcano was almost fully completed during pre-LGM times. Therefore, by the end of the last glaciation (~14 ka), the volcanic cone would have reached its present height. Although González Ferrán (1995) assigns the whole edifice to a postglacial stage, our field observations and geochronological data confirm the

age of Maipo volcano. Postglacial activity on the eastern side of the volcano is restricted to three main episodes: a dacitic bilobate lava flow, an overlying shorter lava flow with similar composition, and summit basandesitic scoria beds.

The calc–alkaline suite depicts a general geochemical trend toward more evolved magmas that potentially are more explosive. However, in detail, cyclic compositional variation can be recognized. In effect, EEI, IV, and VII show a mean silica content of 58%, whereas EEII, III, V, and VI range between 63 and 68% (Fig. 10b). This range is compatible with the periodic tapping of a zoned magma chamber at different depths.

Maipo lavas commonly display disequilibrium textures. The ubiquitous sieve texture in plagioclase (Figs. 5c–d and 6d and e), crystal roundness, and loss of euhedrality in plagioclase and pyroxene (Figs. 5f and 6b) may be explained as partial melting of the mineral phases in response to sudden

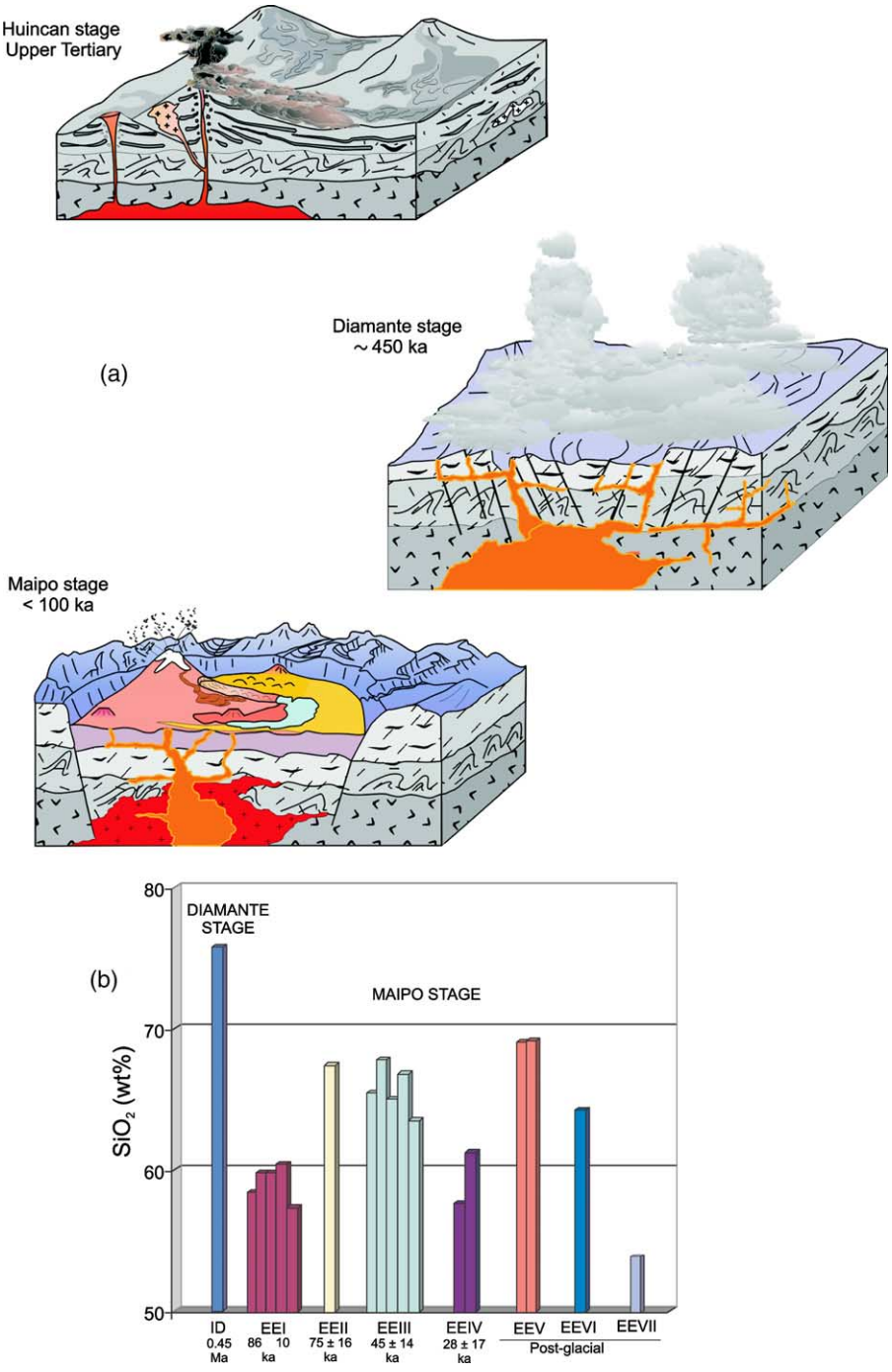

Fig. 10. (a) Schematic evolution of the DMC since Upper Tertiary times. (b) SiO_2 versus time diagram shows general geochemical trend for the DMC and cyclic compositional variation for Maipo stage lavas.

heating by the input of a more mafic batch of magma (Hibbard, 1995). Particularly, 'spongy cellular plagioclase' is considered compatible with magma mixing. Other recognized textures, such as resorption in pyroxene (Fig. 6c), opacite rims in hornblende (Fig. 5b), reaction rims in olivine (Fig. 6f), and zonation in plagioclase and pyroxene are additional indicators of magmatic disequilibrium, compatible with either a sudden decrease in total pressure during rapid magma ascent or magma mixing.

Magma mixing is frequently invoked in Andean volcanoes of the central volcanic zone (De Silva et al., 1993) and SVZ (Hildreth and Moorbath, 1988; Tormey et al., 1995). In most cases, the described disequilibrium textures, such as sieve plagioclase, reaction rims in pyroxenes, and hornblende resorption, are similar to those found in Maipo lavas. Additional evidence comes from the complex zoning of the plagioclase, their mixed matrix and phenocryst composition, mixed hornblende populations, mixed glass composition, and the diagnostic presence of mafic inclusions.

Petrographic and geochemical evidence indicate a model in which an ongoing differentiating system, strongly controlled by fractional crystallization, is periodically injected by deep mafic magma. Although the relative importance of magma mixing in Maipo lavas must be investigated further, the observed disequilibrium textures and cyclic compositional variation support the influence of this process. The absence of mingled pyroclasts suggests that magma injection was followed by full hybridization, which inhibited explosive eruptions.

During the Maipo evolution, no phreatomagmatic eruptions were recorded, which indicates that no interaction with an external source of water occurred. However, progressive cooling and an increase in the differentiation degree may have led to an increase in melt viscosity, which would favor the formation of silicic domes and subsequent pyroclastic flows after dome collapse. As differentiation proceeds toward an increase in water and silica content, the hazard of pyroclastic eruptions is potentially higher. However, a repetition of a Diamante-like catastrophic event, though not impossible, seems highly improbable according to the small magma volume erupted in the last 100 ka. Large magma volumes at the source and a long period of quiescence generally are required to accumulate large volume rhyolitic magma and replenish a shallow magma chamber. The inferred size of the magma chambers in Diamante and Maipo stages would indicate a postglacial trend toward small volume, differentiated products (Fig. 10a).

Petrological evolution may be an useful tool to predict the future behavior of the DMC, with no signs of activity at present. For example, in the Colima volcano of México, the 'petrological monitoring' appears very accurate and successful in eruption prediction (Luhr, 2002).

In the future, much more work must be done. Critical parameters (P, T, water content) must be accurately established for each eruptive event. Microprobe studies on mineral assemblages are necessary to constrain the chemical changes that operated during the evolution of Maipo magmas. Also, isotopic analysis would help constrain the petrogenetic model. Finally, detailed volatile studies are required to understand the degassing system.

6. Concluding remarks

Fieldwork, supported by Ar/Ar ages, indicates that the Maipo volcano has been built almost entirely in a pre-LGM stage. Postglacial activity is volumetrically irrelevant but seems significant in the volcanologic evolution. Historic status is argued until historic activity can be proved with certainty. From the accepted record, the 1822 and 1826 eruptions may be discarded, the 1905 activity remains uncertain, and the 1912 episode is correlated with EEVII. Therefore, the proposed status for the Maipo volcano is potentially active but possibly historic.

Petrographic and geochemical data indicate a trend toward a higher degree of differentiation in terms of time and cyclic compositional variation among Maipo lavas. Fractional crystallization of plagioclase, sanidine, ortho and clinopyroxene, and minor hornblende likely appears as the main control in compositional variation. Disequilibrium textures suggest a subordinate influence of magma mixing as a consequence of periodic injection of mafic magma at the roots of an ongoing differentiation system.

In case of reactivation, future behavior will be closely related to variations in temperature, viscosity, and interaction with external water. Understanding the petrological evolution and the characteristics of the degassing system are critical to hazard assessment.

Acknowledgements

This study was funded by the Agencia Nacional de Promoción Científica y Tecnológica (PMT-PICT0451). The authors appreciate field support from SEGEMAR. Thoughtful reviews by H. Moreno and C. Risso improved the manuscript in form and substance.

References

Barazangui, M., Isacks, B.L., 1976. Spatial distribution of earthquakes and subduction of the Nazca Plate beneath South America. Geology 4, 686–692.

Bühler, M., Pérez, D., Ramos, V.A., 1996. El Jurásico de las nacientes del río Colorado, Departamento de San Carlos, Provincia de Mendoza. In: Xlll Congreso Geológico Argentino, Buenos Aires, Actas, vol. 5, p. 183.

Bühler, G.M., 1997. Geología de las nacientes del río Colorado y del arroyo Durazno, Provincia de Mendoza. Unpublished Thesis. Universidad de Buenos Aires, Buenos Aires.

Charrier, R., 1984. Areas subsidentes en el borde occidental de la cuenca tras-arco jurásico -cretácica, Cordillera Principal chilena entre 34° y 34° 30'S. In: IX Congreso Geológico Argentino, Bariloche, Actas, vol. 2, pp. 107–124.

Clapperton, C., 1993. Quaternary geology and Geomorphology of South America. Elsevier, Amsterdam.

De Silva, S.L., Davidson, J.P., Croudace, I.W., Escobar, A., 1993. Volcanological and petrological evolution of Volcan Tata Sabaya, SW Bolivia. Journal of Volcanology and Geothermal Research 55, 305–335.

Denton, G.H., Heusser, C.J., Lowell, T.V., Moreno, P.J., Andersen, B.G., Heusser, L.E., Schluchter, C., Marchant, D.R., 2000. Interhemispheric linkage of paleoclimate during the last glaciation. Geografiska Annaler-81A, 107–153.

Espizúa, L., 1993. Glaciaciones cuaternarias. In: Ramos, V.A. (Ed.), Geología y Recursos Naturales de Mendoza XII Congreso Geológico Argentino y II Congreso de Exploración de Hidrocarburos, Relatorio, pp. 195–203.

Frey, F.A., Gerlach, D.C., Hickey, R., Lopez-Escobar, L., Munizaga, F., 1984. Petrogenesis of the Laguna del Maule volcanic complex, Chile. Contributions to Mineralogy and Petrology 88, 133–149.

González, F., 1995. Volcanes de Chile. Instituto Geográfico Militar, Santiago de Chile p. 640.

Guerstein, P.G., 1990. Volume estimation of pyroclastic flow deposits through specific area of accumulation. An Andean Example. International Volcanology Congress (Mainz), Abstracts, pp. 41.

Guerstein, P.G., 1993. Origen y significado geológico de la Asociación Piroclástica Pumícea. Pleistoceno de la provincia de Mendoza entre los 33° 30′ y 34° 40′ L.S. Unpublished Ph Thesis. Universidad Nacional de La Plata, La Plata.

Harrington, R., 1989. The Diamante Caldera and Maipo Caldera complex in the Southern Andes of Argentina and Chile (34° 10′ south). Revista de la Asociación Geológica Argentina 19 (1-4), 186–193.

Hibbard, M.J., 1995. Petrography to Petrogenesis. Prentice Hall, Englewood Cliffs, NJ, USA p. 587.

Hildreth, W., Moorbath, S., 1988. Crustal contributions to arc magmatism in the Andes of Central Chile. Contributions to Mineralogy and Petrology 98, 455–489.

Irvine, T.N., Baragar, W.R.A., 1971. A guide to the chemical classification of the common volcanic rocks. Canadian Journal of Earth Sciences 8, 523–548.

Le Maitre, R.W., Bateman, P., Dudek, A., Keller, J., Lameyre Le Bas, M.J., Sabine, P.A., Schmidt, R., Sorensen, H., Streckeisen, A., Woolley, A.R., Zanettin, B., 1989. A Classification of Igneous Rocksand Glossary of Terms. Blackwell, Oxford.

Legarreta, L., Gulisano, C.A., Uliana, M.A., 1993. Las secuencias sedimentarias jurásico-cretácicas. In: Ramos, V.A. (Ed.), Geología y Recursos Naturales de Mendoza XII Congreso Geológico Argentino y II Congreso Exploración de Hidrocarburos. Relatorio, Buenos Aires, pp. 87–114.

Legarreta, L., Gulisano, C., 1989. Análisis estratigráfico secuencial de la Cuenca Neuquina (Triásico superior–Terciario inferior). In: Chebli, G., Spalletti, L. (Eds.), Cuencas Sedimentarias Argentinas Universidad Nacional de Tucumán, Correlación Geológica Serie, vol. 6, pp. 221–243.

Legarreta, L., Uliana, M.A., 1991. Jurassic-Cretaceous Marine Oscillations and Geometry of Back-arc Basin Fill, Central Argentine Andes Special Publication, 12. International Association of Sedimentology, London pp. 429–450.

Lipman, xx, 2000. Calderas. In: Sigurdsson, G. (Ed.), Encyclopedia of Volcanoes. Academic Press, New York.

López Escobar, L., 1984. Petrology and chemistry of volcanic rocks of the southern Andes. In: Harmon, R.S., Barreiro, B. (Eds.), Andean Magmatism, Chemical and Isotopic Constraints. Shiva Publ Co, Cambridge, MA, pp. 47–71.

Luhr, J.F., 2002. Petrology and geochemistry of the 1991 and 1998–1999 lava flows from Volcán de Colima, México: implications for the end of the current eruptive cycle. Journal of Volcanology and Geothermal Research 117, 169–194.

Pearce, J.A., 1983. Role of the sub-continental lithosphere in magma genesis at active continental margins. In: Hawkesworth, C.J., Norry, M.J. (Eds.), Continental Basalts and Mantle Xenoliths. Shiva, Cambridge, MA, pp. 230–249.

Pereyra, F.X., 1996. Geomorfología. In: Ramos, V.A. (Ed,) Geología de la región del Aconcagua, provincias de San Juan y Mendoza. Subsecretaría de Minería de la Nación. Dirección Nacional del Servicio Geológico. Anales 24 (15): 423–446, Buenos Aires.

Pérez, D.J., Alvarez, G., Concheiro, A., Ramos, V.A., 1997. La Formación Papal: depósito sinorogénico de la cuenca de antepaís de Tunuyán, Mendoza, Argentina. In: VIII Congreso Geológico Chileno, Antofagasta, Actas, vol. 1, pp. 568–571.

Polanski, J., 1964. Descripción geológica de la Hoja 26c, La Tosca. Dirección Nacional Geología y Minería, Boletín 101, Buenos Aires.

Ramos, V.A., Godoy, E., Giambiagi, L., Aguirre - Urreta, M.B., Alvarez, P.P., Pérez, D.J., Tunik, M., 1998. Tectónica de la Cordillera Principal en la región del volcán san José (34° LS), provincia de Mendoza, Argentina. In: X Congreso Latinoamericano de Geología y VI Congreso Nacional de Geología Económica, Buenos Aires, Actas, vol. 2, p. 104.

Ramos, V.A., 1988. The tectonics of the Central Andes (30°-33°S latitude). In: Clark, S., Burchfiel, D., Suppe, J. (Eds.). Processes in continental lithospheric deformation, Geological Society of America, Boulder, Special Paper 218, pp. 31–54.

Siebert, L., Simkin, T., 2002. Volcanoes of the World:an Ilustrated Catalog of Holocene volcanoes and their eruptions. Smithsonian Institution, Global Volcanism Program Digital Information Series GVP-3 (http:www.volcano.si.edu/gvp/world/).

Sruoga, P., Fauqué, L., Llambías, E.J., 1998. ¿Es el Volcán Maipo (34° 10′S, 69° 52′O) un centro activo?. In: X Congreso Latinoamericano de Geología y VI Congreso Nacional de Geología Económica, Buenos Aires, Actas, vol. 1, pp. 131–136.

Sruoga, P., Llambías, E., Fauqué, L., 2000. Geocronología y evolución geoquímica del volcán Maipo (34° 10′S). In: IX Congreso Geológico Chileno, Puerto Varas, Actas, vol. 2. pp. 72–76.

Stauder, W., 1973. Mechanism and spatial distribution of Chilean earthquakes with relation to subduction of the oceanic plate. Journal of Geophysical Research 78, 5033–5061.

Stern, C.R., Amini, H., Charrier, R., Godoy, E., Hervé, F., Varela, J., 1984. Petrochemistry and age of rhyolitic pyroclastic flows which occur along the drainage valleys of the río Maipo and río Cachapoal (Chile) and the río Yaucha and río Papagayos (Argentina). Revista Geológica de Chile 23, 39–52.

Stipanicic, P.N., Rodrigo, F., 1970. El diastrofismo jurásico en Argentina y Chile. In: IV Jornadas Geológicas Argentinas, Actas, vol. II, pp. 353–368.

Taylor, S.R., McLennan, S.M., 1985. The Continental Crust: Its Composition and Evolution. Blackwell, Oxford.

Tormey, D.R., Hickey-Vargas, R., Frey, F. and López-Escobar, L., 1991. Recent lavas from the Andean volcanic front (33 to 42°S); interpretations of along-arc compositional variations. Geological Society of America. Special Paper 265, 57–77.

Tormey, D.R., Frey, F., López-Escobar, L., 1995. Geochemistry of the active Azufre-Planchón-Peteroa Volcanic Complex, Chile (35°15′S): evidence for multiple sources and processes in a Cordilleran arc magmatic system. Journal of Petrology 38 (2), 265–298.